Journal of the Korean Physical Society
https://doi.org/10.1007/s40042-025-01392-9

Online ISSN 1976-8524
Print ISSN 0374-4884

RESEARCH - FLUIDS, PLASMAS AND PHENOMENOLOGY

Numerical investigation of the effect of high-voltage frequency on the density of RONS species in the air atmospheric pressure gas discharge

Fariborz Momtazzadeh[1] · Farshad Sohbatzadeh[1,2] · Hamed Soltani Ahmadi[1,2] · Ramin Mehrabifard[3]

Received: 17 January 2025 / Revised: 19 April 2025 / Accepted: 8 May 2025

Abstract
In the last few decades, studies in various fields of plasma technology have expanded and its application in different processes has increased. Therefore, the achievement of a desirable and practical plasma with specific characteristics is of particular importance. The frequency of the applied voltage is one of the important factors that play a role in the physical and chemical characteristics. In this research, changes in the density of active species produced in an electrical discharge using a dielectric barrier and air working gas have been investigated, from a frequency of 500 Hz to 500 kHz, and by applying a constant voltage of 2 kV, have been investigated. For this purpose, 87 different reactions with specific collision cross-sections were defined in COMSOL Multiphysics. Other parameters, including current–voltage waveform, electric field, species density including NO, OH, O_2^+, O_3, etc., were evaluated. The results show that under completely identical conditions, the electron temperature distribution changes with increasing applied frequency, and the density of reactive oxygen and nitrogen species (RONS) like (NO, OH, O_2,..) decreases, but O_2^+ shows an increasing trend. It should be noted that the simulation results are in good agreement with the previous experimental and simulation reports. These results offer valuable insights into optimizing plasma parameters for different applications, potentially resulting in better treatment outcomes across a range of therapeutic domains.

Keywords Cold atmospheric pressure plasma · Dielectric barrier discharge · RONS · High voltage frequency · COMSOL multiphysics · Gas discharge

1 Introduction

Atmospheric pressure cold plasma, as an innovative technology, has diverse applications in various fields, surface treatment [1], water decontamination [2], and many applications in medicine [3], including killing bacteria [4], cancer cell treatment [5–7], and so on. Plasma is a quasi-neutral gas composed of positive and negative ions, free radicals, UV radiation, and other particles, with approximately equal charge density [8, 9]. Since the ionization process typically starts at a specific temperature, usually several thousand Kelvins, plasma is often referred to as the fourth state of matter [10]. It is important to note that not all ionized gases can be classified as plasma, as specific conditions must be met for a state to be defined as plasma.

One method of plasma generation involves the electrical discharge of various gases using a dielectric barrier, which is achieved by applying the appropriate voltage in different frequency ranges (with sufficient injected power) [11].

The electron is freed first from the atoms and molecules by natural background radiation, cosmic rays, or thermionic emission, and then, the electron gets accelerated by the electric field. Accelerated electrons produce ionized atoms and molecules. The plasma generated by gas discharge possesses unique characteristics that determine its applications in different fields. Therefore, investigating the physical and chemical parameters of plasma under various conditions is crucial to design an optimized plasma reactor tailored to specific applications [12].

✉ Hamed Soltani Ahmadi
hamedsoltani1991@gmail.com

[1] Department of Atomic and Molecular Physics, Faculty of Basic Sciences, University of Mazandaran, Babolsar 47416-95447, Mazandaran, Iran

[2] Plasma Technology Research Core, Faculty of Science, University of Mazandaran, Babolsar, Iran

[3] Division of Environmental Physics, Faculty of Mathematics, Physics and Informatics, Comenius University, Mlynska dolina, Bratislava 842 48, Slovakia

Published online: 15 May 2025

Simulation is a method wherein a computer model of a real or hypothetical system is developed to analyze its behavior under varying situations [13]. These models can simulate physical, chemical, biological, or even social phenomena, and are used for predicting outcomes, optimizing processes, and training purposes [14]. Simulations are widely used in engineering, medicine, economics, and social sciences [15]. This method allows users to analyze desired results without the need for real and costly experiments [16].

COMSOL is one of the most advanced and comprehensive simulation tools in the fields of science and engineering. This software, as a comprehensive and advanced package to simulate complex systems, is capable of solving differential equations of nonlinear systems using partial derivatives using the Finite Element Method (FEM) in various spatial dimensions, including zero, one, two, and three dimensions, accurately and effectively [17].

In recent years, extensive studies have been conducted on the simulation of dielectric barrier discharge (DBD) [18–20]. For example, in 2002, Golubovskii and colleagues performed a numerical simulation on helium plasma and calculated various plasma parameters under constant conditions [14]. In 2009, Petrovic et al. conducted a two-dimensional simulation of cylindrical DBD with helium gas mixed with nitrogen impurities [15]. In 2013, Rokeya and colleagues performed a one-dimensional simulation for DBD with helium gas, analyzing the effects of dielectric constant and electrode spacing [16]. In 2017, Gadkari and colleagues simulated a coaxial cylindrical DBD plasma in pure helium gas using a two-dimensional fluid model in COMSOL [17]. Furthermore, in previous study in our group, a one-dimensional simulation in COMSOL performed and useful plasma parameters calculated [18]. We also investigated the effect of humidity on helium discharge and its effect on RONS production [21].

This study numerically examines the effect of changing the applied high-voltage frequency in atmospheric pressure electrical discharge on the density of active oxygen and nitrogen species in air. Determining useful parameter values experimentally is not cost-effective; thus, simulating an air gas discharge system using a dielectric barrier within a frequency range of 500 Hz to 500 kHz is necessary. This simulation examines parameters, such as species density, voltage-current characteristics, electric field distribution, electron temperature distribution, average species energy distribution, etc. The specific frequencies analyzed in this simulation are 500 Hz, 50 kHz, and 500 kHz. A significant observation is the decline of some species with increasing frequency. The goal of our study is to highlight the dynamic features of the ignition phase and examine how discharge characteristics vary with frequency in this early stage.

2 Simulation procedure

In this section, the simulation of dielectric barrier discharge in the presence of a nitrogen gas is described. This simulation allows us to analyze and examine key variables, such as species density, potential and electric field, electron temperature, and other related parameters. To achieve this simulation, we decided to include various gases as additives to the nitrogen gas. This process involves a detailed examination of the reactions between these gases and electrons with the species present in the discharge phenomenon.

2.1 Electrical discharge simulation between two electrodes

To achieve the objectives of the present investigation, the dielectric barrier discharge simulation was carefully performed at 1 atmosphere pressure and 400 Kelvin temperature. Our goal is to create an accurate simulation of electrical discharge in the presence of oxygen and nitrogen gases, which are known for their reactive oxygen and nitrogen species (RONS). In this regard, we initially used pure nitrogen gas (N_2) and then considered the use of air, which is a mixture of nitrogen and oxygen. These gases were placed between two parallel plates, and then, by applying a sinusoidal alternating voltage, the necessary conditions for plasma generation were established. This process not only leads to plasma production, but also accurately displays the physical behaviors and chemical reactions in various environments under simulated conditions. Although the process of simulating electrical discharge in two dimensions may be practical and feasible, some challenges and issues arising from this approach lead us to choose an alternative. One of the main problems is the increased simulation time and the greater complexity and difficulty in interpreting and analyzing the results. For this reason, our preference and interest shift toward using a one-dimensional simulation, as this method can be more efficient. To perform the desired electrical discharge simulation, we used version 6.1 of the COMSOL software. In this program, we used the plasma module, which is specifically designed for modeling plasma phenomena. Additionally, for greater accuracy and more detailed analysis, we utilized the Plasma-Plas submodule. After selecting a sinusoidal voltage for the power electrode, it is necessary to correctly define and input the time-dependent behavior of the electrical discharge process. To perform this, in the software, we navigated to the study section and selected the Time-Dependent option.

2.2 Geometry and meshing

The geometry used in this study is one-dimensional (line and points). The COMSOL software employs the Finite Element Method (FEM) strategy. Figure 1 illustrates the geometry and boundary conditions of the air–gas discharge system using a dielectric barrier.

The geometry of the system includes two electrodes (power and ground), two dielectrics, the plasma formation region, and the surface reactions at the walls. The starting and ending points of our design clearly represent the two electrodes (1 and 4), whereas the distance between these electrodes, along with their opposing points, forms our dielectric (between 1 and 2, between 3 and 4). The intermediate space, located between the two dielectrics, is referred to as the gap region, where all the essential and vital reactions in this system take place (between 2 and 3). The distance between the two electrodes is precisely set at 3 mm, while the gap length is determined to be 1 mm. The dielectrics used in this design are 1 mm long and have a considerable thickness of 1 mm. Figure 2 presents a two-dimensional schematic of the geometry of the system.

The point-based meshing (networking) used in simulation is discussed in this study. The COMSOL software uses FEM to decompose complex problems into smaller, more solvable components. To achieve balance, we use a variable-density meshing approach. In areas where events are of greater significance, we use finer meshing to model more details (minimum element size = 6E−4 [mm]). Conversely, in more distant and less critical regions, we use larger elements (maximum element size = 3E−2 [mm]), which help reduce the overall computational load. Figure 3 shows an overall view of the meshing used in this study, which appears uniform due to the large number of elements. Moreover, Table 1 presents the general features of the meshing.

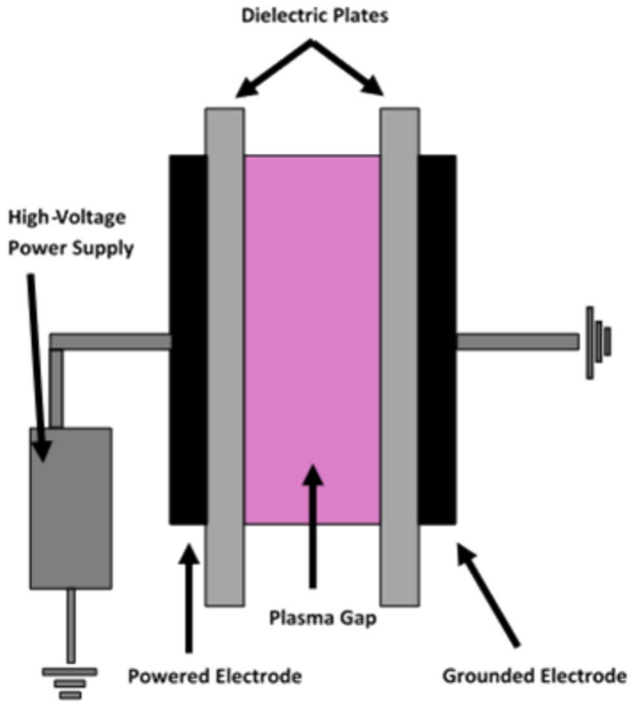

Fig. 2 Two-dimensional diagram of the system geometry

2.3 Reactions and parameters

Air is made up of 78% nitrogen and 21.5% oxygen, with the rest being various gases, including moisture, which we consider to be air vapor (0.5%). In this study, 87 reactions

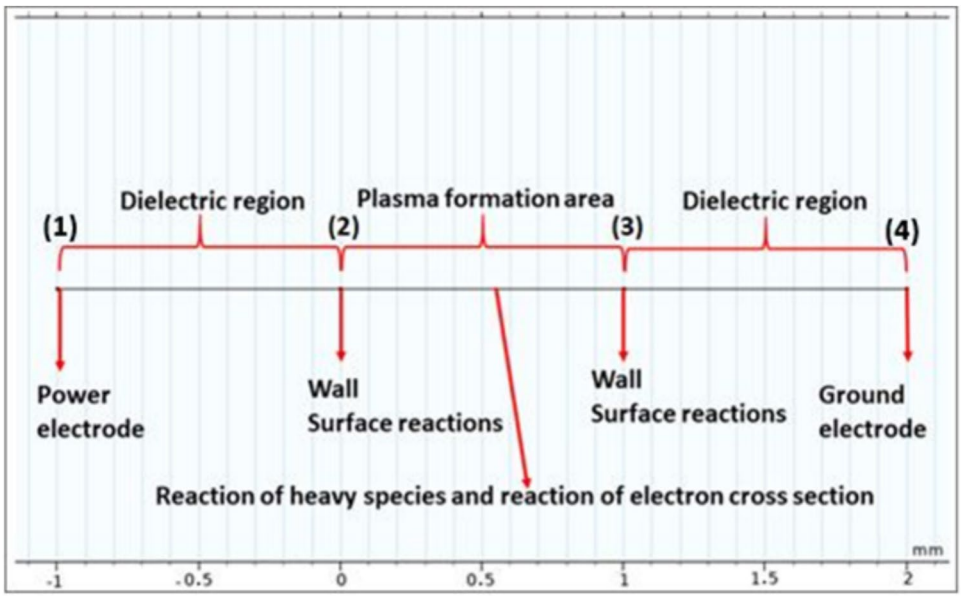

Fig. 1 Schematic of the system geometry and boundary conditions

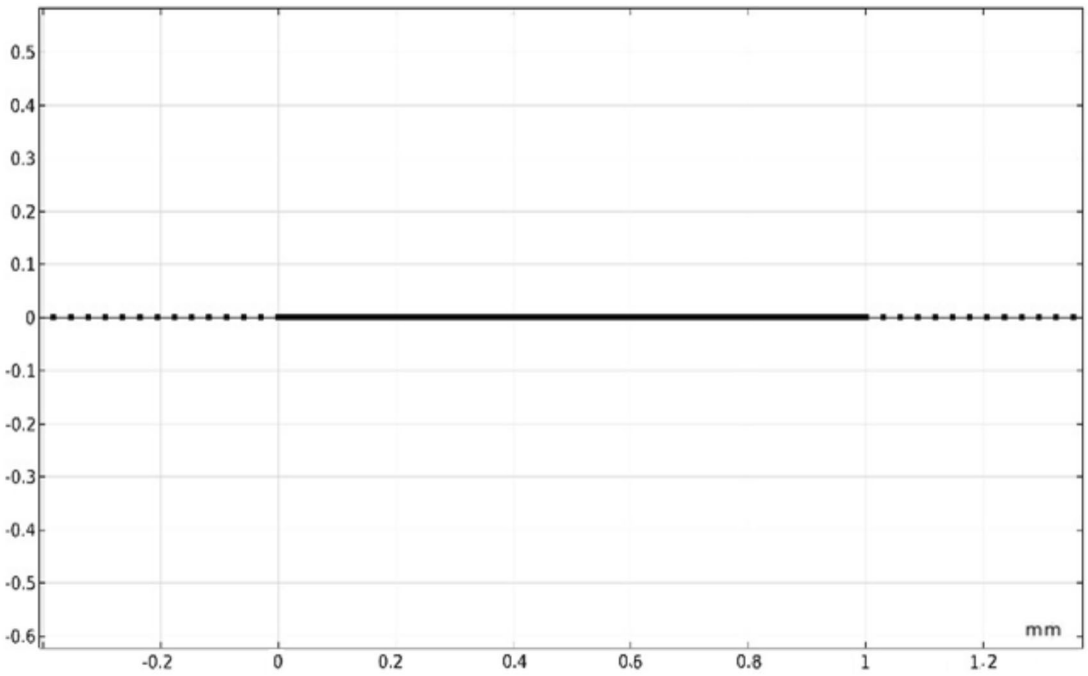

Fig. 3 Schematic of the meshing of the system

Table 1 General features of the meshing

Description	Value
Maximum element size	3E−2 [mm]
Minimum element size	6E−4 [mm]
Curvature factor	0.2
Predefined size	Extremely fine

between heavy species and electron reactions with neutral species in the plasma region, as well as other surface reactions for secondary electron emission and plasma stability in the wall region, were defined. In line with the conducted research, nitrogen gas was first introduced into the gap region, followed by air gas. Under the specific conditions present, these gases undergo various electrochemical and physical reactions in the region of interest.

Table 2 clearly shows the electron impact reactions in detail for the species present in the nitrogen gas discharge state. This table represents electron impact reactions with nitrogen molecules, N_2s (excited nitrogen), and N_2^+ (one-ionized nitrogen).

By inputting the electron collision cross-section data and its energy in each of the aforementioned states, which were provided as inputs to the software, accurate values of species density and other important information will be obtained. Other reactions occurring in the nitrogen gas discharge N_2 in the specified gap are shown in Table 3. For these reactions, the software receives a rate constant, denoted as K^f, as input, and these reactions are considered irreversible.

In the Table 3, N^+ denotes a singly ionized nitrogen atom, N_2^+ denotes a singly ionized nitrogen molecule, and N denotes a nitrogen atom.

Additionally, other reactions known as surface reactions are defined at the wall boundary (boundaries 2 and 3 in Fig. 1). In these reactions, the ionized and excited species combine with electrons and return to their neutral state. Table 4 presents the essential surface reactions for simulating the electric discharge of nitrogen gas in a comprehensive and accurate manner.

To simulate the electric discharge in air, we require more complex processes that involve additional reactions. These reactions include the effect of electrons on oxygen species as well as interactions between nitrogen, oxygen, and water vapor species. The oxygen species, due to their high reactivity, are considered one of the key factors in this system. Table 5 shows the electron impact reactions on oxygen molecules for the electric discharge simulation in air.

Next, in Table 6, other reactions required to simulate the electrical discharge of air gas between two dielectrics are presented:

In Table 6, O_2 represents an oxygen molecule, O_3 represents an ozone molecule, O represents an oxygen atom, O_2^+ represents a singly positively charged oxygen molecule, O_2^- represents a singly negatively charged oxygen molecule, H_2O represents water vapor, NOx compounds (NO, NO_2,

Table 2 Electron impact reactions [18, 22, 23]

Reaction	Formula	Type	ΔE(ev)
1	$e + N_2 \rightarrow e + N_2$	Elastic	–
2	$e + N_2 \rightarrow e + N_2s$	Excitation	0.02
3	$e + N_2 \rightarrow e + N_2s$	Excitation	0.29
4	$e + N_2 \rightarrow e + N_2s$	Excitation	0.291
5	$e + N_2 \rightarrow e + N_2s$	Excitation	0.59
6	$e + N_2 \rightarrow e + N_2s$	Excitation	0.88
7	$e + N_2 \rightarrow e + N_2s$	Excitation	1.17
8	$e + N_2 \rightarrow e + N_2s$	Excitation	1.47
9	$e + N_2 \rightarrow e + N_2s$	Excitation	1.76
10	$e + N_2 \rightarrow e + N_2s$	Excitation	2.06
11	$e + N_2 \rightarrow e + N_2s$	Excitation	2.35
12	$e + N_2 \rightarrow e + N_2s$	Excitation	6.17
13	$e + N_2 \rightarrow e + N_2s$	Excitation	7
14	$e + N_2 \rightarrow e + N_2s$	Excitation	7.35
15	$e + N_2 \rightarrow e + N_2s$	Excitation	7.8
16	$e + N_2 \rightarrow e + N_2s$	Excitation	8.4
17	$e + N_2 \rightarrow e + N_2s$	Excitation	8.16
18	$e + N_2 \rightarrow e + N_2s$	Excitation	8.55
19	$e + N_2 \rightarrow e + N_2s$	Excitation	8.89
20	$e + N_2 \rightarrow e + N_2s$	Excitation	11.03
21	$e + N_2 \rightarrow e + N_2s$	Excitation	11.88
22	$e + N_2 \rightarrow e + N_2s$	Excitation	12.25
23	$e + N_2 \rightarrow e + N_2s$	Excitation	13
24	$e + N_2 \rightarrow 2e + N_2^+$	Ionization	15.6
25	$e + N_2 \rightarrow e + N_2a3s$	Excitation	6.72
26	$e + N_2a3s \rightarrow e + N_2$	Excitation	−6.72
27	$e + N_2 \rightarrow e + N + N$	Excitation	8
28	$e + H_2O \rightarrow e + H + OH$	Excitation	7.1

and NO_3), and N^+ represents a singly positively charged nitrogen atom.

2.4 Initial parameters

The measurement system in this simulation is SI. The simulation was carried out at three frequencies: 500 Hz, 50 kHz, and 500 kHz, with an applied peak-to-peak voltage of 2 kV. The diameter of the plate was set at 0.1 m. The initial parameters which show in Table 7 were entered in the Initial Values section of the Plasma module. The time step was chosen as 1×10^{-5} for 500 Hz, 1×10^{-7} for 50 kHz, and 1×10^{-8} for 500 kHz.

2.5 Physics and equations

Now, we add surface reactions to the model; these reactions specifically describe the neutralization of ions on the electrodes. To ensure the stability of the electrical discharge, the presence of secondary electron emission is essential. Therefore, it is necessary to specify and input the emission coefficient and an estimate of the average energy of secondary electrons based on the ionization threshold energy and the metal surface's work function. For these reactions to make sense, a wall must be defined; therefore, boundaries 2 and 3, as shown in Fig. 1, will act as the wall. However, an important point in the simulation process is that plasma-related problems must be solved under electrically neutral initial conditions. To this end, in the nitrogen ion species section (species: N_2), the option "Initial Value from Electroneutrality Constraint" is enabled for both electrical discharge simulation scenarios.

Part of the equations includes the drift–diffusion equations solved for each species, such as electrons, positive ions, and negative ions. Equations 1 and 2 represent the electron transport and the sources of electron production and loss, respectively

$$\frac{\partial n_e}{\partial t} + \nabla.\left(-\overrightarrow{D_e}\nabla n_e - \overrightarrow{\mu_e}\vec{E}n_e\right) - R_e = 0, \tag{1}$$

$$R_e = \sum_{j=1}^{M} x_j \alpha_j N_n \left|\Gamma_e\right|, \tag{2}$$

where, in Eq. (1), the electron density, mobility, and diffusion coefficient are denoted as n_e, μ_e, and D_e respectively. The electric field vector and the electron production and loss source term are represented by $\vec{E}$ and R_e, respectively. Equation (3), known as the Poisson equation, represents the electric field distribution in the region between two electrodes also calculates the electrostatic field

Table 3 Other gap space reactions for nitrogen gas discharge [18]

Reaction	Formula	Type	Rate constant $K^f\left(m^3/s.mol\right)$
1	$e + N^+ \rightarrow N$	Recombination	3.5×10^{-18}
2	$e + N_2 \rightarrow 2e + N + N^+$	Dissociative ionization	2.4×10^{-23}
3	$e + N_2 \rightarrow 2N$	Dissociative	2×10^{-17}
4	$e + N_2^+ \rightarrow 2N$	–	2.8×10^{-13}
5	$N^+ + N_2 \rightarrow N + N_2^+$	Charge exchange	10^{-17}

Table 4 Surface reactions required in air discharge simulation [18]

Reaction	Formula	Sticking coefficient
1	$O_2s \rightarrow O_2$	1
2	$O_2a1d \rightarrow O_2$	1
3	$O_2b1s \rightarrow O_2$	1
4	$O_245 \rightarrow O_2$	1
5	$O^- \rightarrow O$	1
6	$O1d \rightarrow O$	1
7	$O1s \rightarrow O$	1
8	$N_2^+ \rightarrow N_2$	1
9	$N_2a3s \rightarrow N_2$	1

Table 5 Electron impact reactions on oxygen molecules [22, 23]

Reaction	Formula	Type	ΔE(ev)
1	$e + O_2 \rightarrow e + O_2$	Elastic	–
2	$e + O_2 \rightarrow O + O^-$	Attachment	–
3	$e + O_2 \rightarrow e + O_2$	Excitation	0.02
4	$e + O_2 \rightarrow e + O_2$	Excitation	0.19
5	$e + O_2 \rightarrow e + O_2$	Excitation	0.19
6	$e + O_2 \rightarrow e + O_2$	Excitation	0.38
7	$e + O_2 \rightarrow e + O_2$	Excitation	0.38
8	$e + O_2 \rightarrow e + O_2$	Excitation	0.57
9	$e + O_2 \rightarrow e + O_2$	Excitation	0.75
10	$e + O_2 \rightarrow e + O_2a1d$	Excitation	0.977
11	$e + O_2a1d \rightarrow e + O_2$	Excitation	−0.977
12	$e + O_2 \rightarrow e + O_2b1s$	Excitation	1.627
13	$e + O_2b1s \rightarrow e + O_2$	Excitation	−1.627
14	$e + O_2 \rightarrow e + O_245$	Excitation	4.5
15	$e + O_245 \rightarrow e + O_2$	Excitation	−4.5
16	$e + O_2 \rightarrow e + O + O$	Dissociative	6
17	$e + O_2 \rightarrow e + O + O1d$	Excitation	8.4
18	$e + O_2 \rightarrow e + O1s$	Excitation	9.97
19	$e + O_2 \rightarrow 2e + O_2^+$	Excitation	12.06

$$\nabla.\left(\varepsilon_0\varepsilon_r\vec{E}\right) = \rho, \tag{3}$$

where ε_0, ε_r, and ρ represent the permittivity of the free space, the relative dielectric constant, and the net charge density of the plasma species, respectively. Equations (4) and (5) represent the secondary emission flux resulting from the collisions of positive and negative ions with the electrode surface, leading to the ejection of electrons from the electrode surface

$$\overrightarrow{\Gamma_e} = \gamma n_n \mu_n \left|\vec{E}\right|, \tag{4}$$

Table 6 Other reactions required in the simulation of electrical discharge in air [18, 19]

Reaction	Formula	Rate constant $K^f\left(m^3/s.mol\right)$
1	$O + O_2 + O_2 \rightarrow O_3 + O_2$	$6 \times 10^{-46} \times \left(1.3^{-2.8}\right)$
2	$O + O_2 + N_2 \rightarrow O_3 + N_2$	$5.6 \times 10^{-46} \times \left(1.3^{-2.8}\right)$
3	$O + O_3 \rightarrow O_2 + O_2$	$8 \times 10^{-18} \times \exp\left(-2060/40\right)$
4	$N + O_3 \rightarrow NO + O_2$	1×10^{-22}
5	$N_2^+ + N_2 + O_2 \rightarrow N_4^+ + O_2$	18×10^6
6	$N_4^+ + O_2 \rightarrow O_2^+ + N_2 + N_2$	15×10^7
7	$N + O_2 \rightarrow NO + O$	$1.5 \times 10^{-7} \times \exp(8)$
8	$N + NO \rightarrow N_2 + O$	$2.1 \times 10^{-11} \times \exp(0.25)$
9	$2N + NO \rightarrow N_2a3s + NO$	6.1×10^2
10	$O1s + NO \rightarrow O1d + NO$	2.2×10^8
11	$NO + OH + O_2 \rightarrow HNO_2 + O_2$	2.2×10^5
12	$NO + OH + N_2 \rightarrow HNO_2 + O_2$	2.2×10^5
13	$HNO_2 + OH \rightarrow NO_2 + H_2O$	7.8×10^4
14	$NO_2 + H \rightarrow NO + OH$	7.7×10^7
15	$H_2O + O \rightarrow OH + OH$	9.6×10^5
16	$OH + OH \rightarrow H_2O + O$	1.1×10^6
17	$O + OH \rightarrow O_2 + H$	$2.3 \times 10^{-17} \times \exp(0.3)$
18	$OH + O_3 \rightarrow HO_2 + O_2$	4×10^4
19	$OH + HO_2 \rightarrow H_2O + O_2$	4.7×10^7
20	$HO_2 + O \rightarrow OH + O_2$	9×10^6
21	$HO_2 + O_3 \rightarrow OH + O_2 + O_2$	1.2×10^3
22	$H + O_2 + O_2 \rightarrow HO_2 + O_2$	1.9×10^4
23	$H + O_3 \rightarrow OH + O_2$	1.2×10^6
24	$H + O_3 \rightarrow HO_2 + O$	1.2×10^6
25	$H + HO_2 \rightarrow OH + O$	10^7
26	$H + OH \rightarrow NO + H$	1.7×10^7

Table 7 Initial parameters of simulation

Initial parameters	Parameters value
Pressure	760 [Torr]
Temperature	400 [k]
Initial mean electron energy	5 [V]
Initial Electron density	10^{13} [1/m^3]
Electron mobility	Calculation from the electron collision cross-section

$$\overrightarrow{\Gamma_e} = \gamma n_P \mu_P \left|\vec{E}\right|, \tag{5}$$

in which γ represents the secondary emission coefficient.

The electron energy density is represented in Eq. (6), and the energy rate due to inelastic collisions is given in Eq. (7)

$$\frac{\partial n_\varepsilon}{\partial t} + \nabla.\vec{\Gamma}_\varepsilon + \vec{E}.\vec{\Gamma}_e = R_\varepsilon - (\vec{u}.\nabla)n_\varepsilon, \tag{6}$$

$$R_\varepsilon = S_{en} + \frac{Q + Q_{gen}}{q}. \tag{7}$$

In Eq. (7), S_{en} represents the collision power loss ($\frac{W}{m^3}$), Q is the electron heat source (typically due to the magnetic field), Q_{gen} is the main heat source, and q is the electric charge (C). Surface charge accumulation at the boundary of the walls (boundaries 2 and 3)

$$\frac{\partial \sigma_s}{\partial t} = n.J_i + n.j_e, \tag{8}$$

where σ_s, J_i, and j_e are the surface charge density, ionic flux density, and electric flux density, respectively. To calculate σ_s, we have

$$\sigma_s = -n.(D1 - D2). \tag{9}$$

$D1 - D2$ are displacement fields across an interface, multiplied by the surface normal (n).

The continuity Eq. (10) for ion species is as follows:

$$\frac{\partial n_i}{\partial t} + \nabla.(n_i\vec{u}) = -\nabla.(\mu_i n_i q_i \nabla\varphi - D_i \nabla n_i) + S_i. \tag{10}$$

In total, in the equations mentioned above, $\vec{\Gamma}_e$ is the electron flux, R_ε is the energy rate of inelastic collisions,n_ε is the electron energy density, S_i is the ion production source, n_i is the ion density, and φ is the electrostatic potential. According to Fig. 1, for Eqs. (1), (2), (3), (6), (7), and (10), all occur in the boundaries between 2 and 3, in the plasma region. And Eqs. (4) and (5) are used in boundary 2 and 3, which secondary emission will happen. Meanwhile, the boundary conditions of the dielectric region, namely the region between boundaries 1 and 2 and the region between boundaries 3 and 4, were defined as charge conservation.

3 Simulation results and analysis

3.1 Mesh-independent curve

According to the curve plotted in Fig. 4, changes in the mesh elements show little variation in the electric current values at a frequency of 50 kHz and a peak-to-peak voltage of 2 kV.

As can be seen, no changes in the electron temperature values are observed from the default element size of Fine onward. Therefore, in the present study, the Extremely Fine setting was considered by default.

Figure 5 shows the voltage–current waveform at three frequency levels: 500 Hz, 50 kHz, and 500 kHz, with a peak-to-peak voltage of 2 kV. In the voltage–current curve,

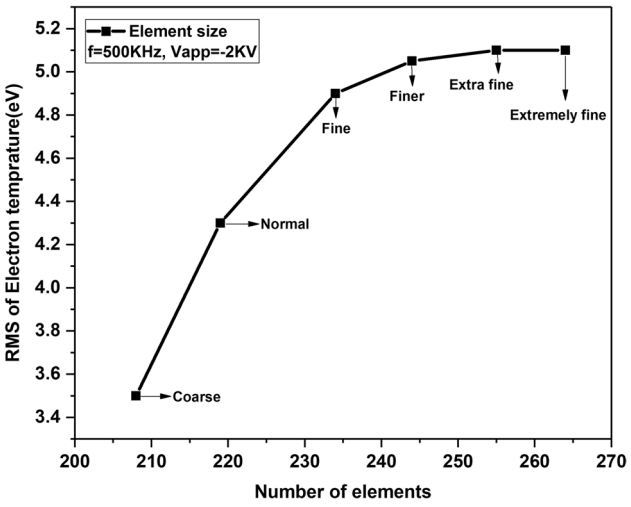

Fig. 4 The mesh-independent curve of the RMS of electron temperature at the center of the plasma discharge gap

the current will change when we use the sinusoidal voltage, according to the collision rate and the time dependence of the plasma equations. At higher frequencies, the plasma experiences rapid charging and discharging of the dielectric barrier, which may lead to unequal current amplitudes and asymmetric waveform shapes during the early cycles. These effects are especially visible during the ignition phase, where the space charge and wall charge distributions are still developing. To have better estimation of concentration of species, we use root mean square (RMS) of two periods in this simulation.

Figures 6, 7, 8 show the logarithmic RMS curves of different distributions at three frequency levels in the plasma region. The reason for plotting the logarithmic curve was that the differences between the curves at certain frequencies were large, and the curve lines either overlapped or were spaced far apart. Another reason was the inability to observe the details. As shown in Fig. 6 higher frequency shows higher temperature and electron density which are 5.5 eV and around 10^{18} ($1/m^3$) in maximum, respectively.

Figures 7 and 8 show concentration of different species with different frequency in plasma reactor, as shown in figures increasing frequency can decreasing density of NO, OH, and O_3, but density of O_2^+ shows an increasing trend toward increasing frequency. At higher frequencies, the electron energy distribution function (EEDF) changes, and ion recombination rates can also change [24]. At higher frequencies, the electric field changes more rapidly, which can result in more energetic electron collisions, increasing the formation of O_2^+ through ionization of O_2 molecules. Reduced densities of other reactive species might indicate that recombination or secondary reactions are more dominant at higher frequencies, or that the plasma

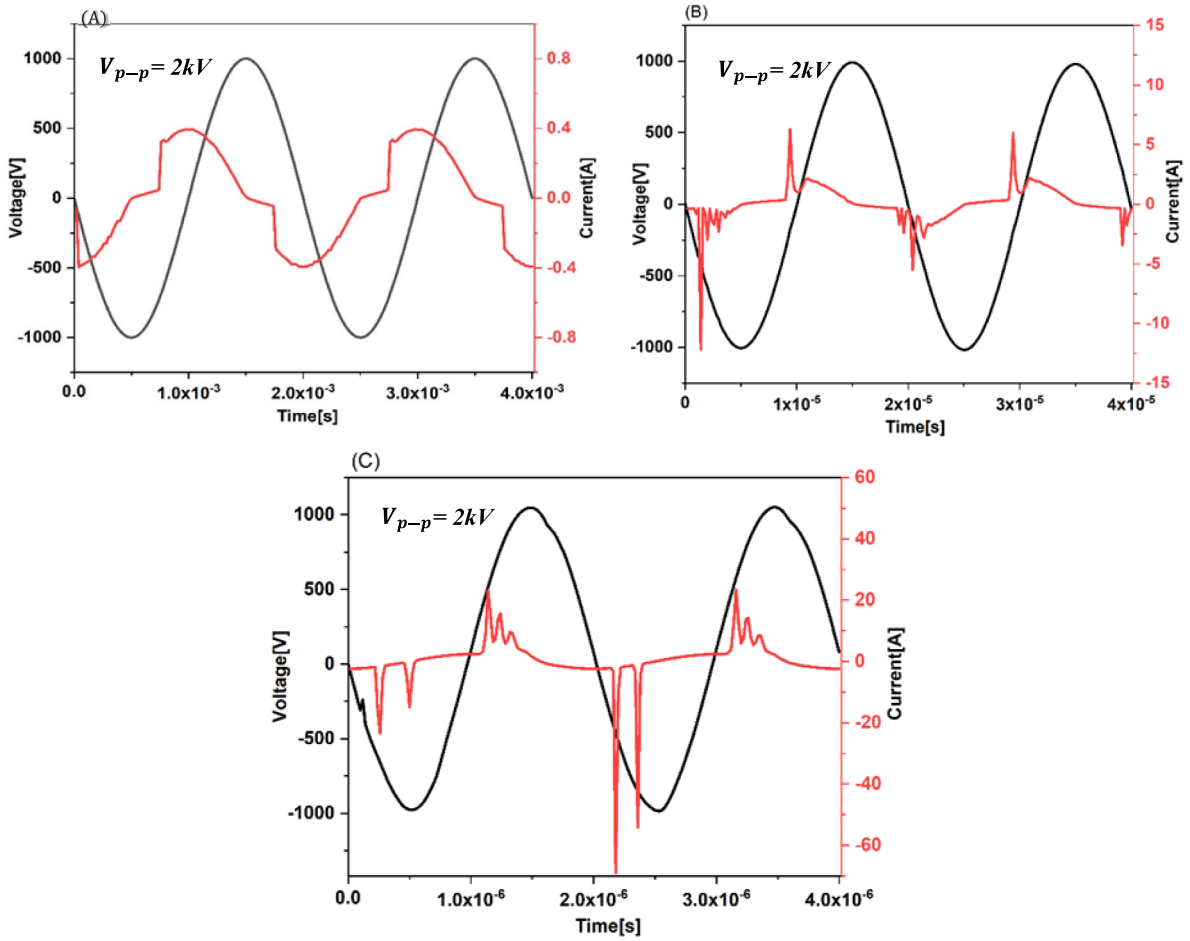

Fig. 5 The V–I characteristic curves at three frequency levels: **A** 500 Hz, **B** 50 kHz, and **C** 500 kHz

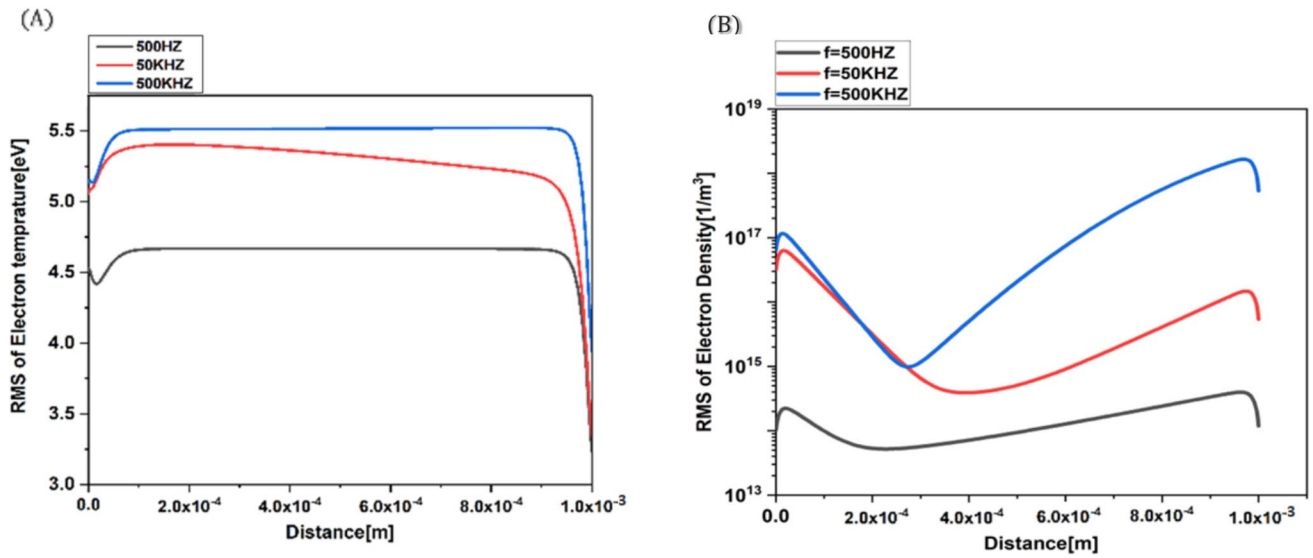

Fig. 6 Logarithmic RMS curves of the **A** electron temperature and **B** electron density distributions at three frequency levels in the plasma region

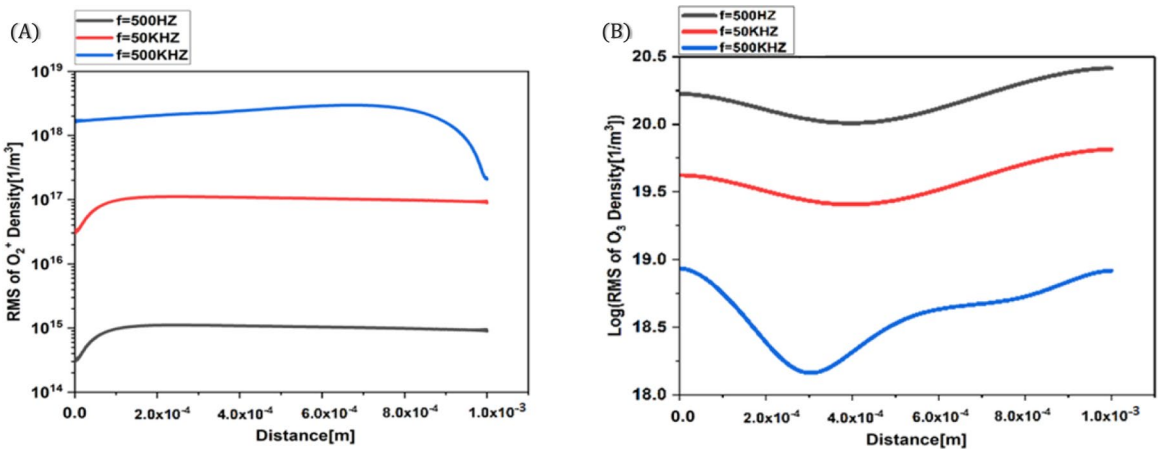

Fig. 7 The RMS curve of the **A** O_2^+ ion density distribution and the **B** O_3 species at three frequency levels in the plasma region

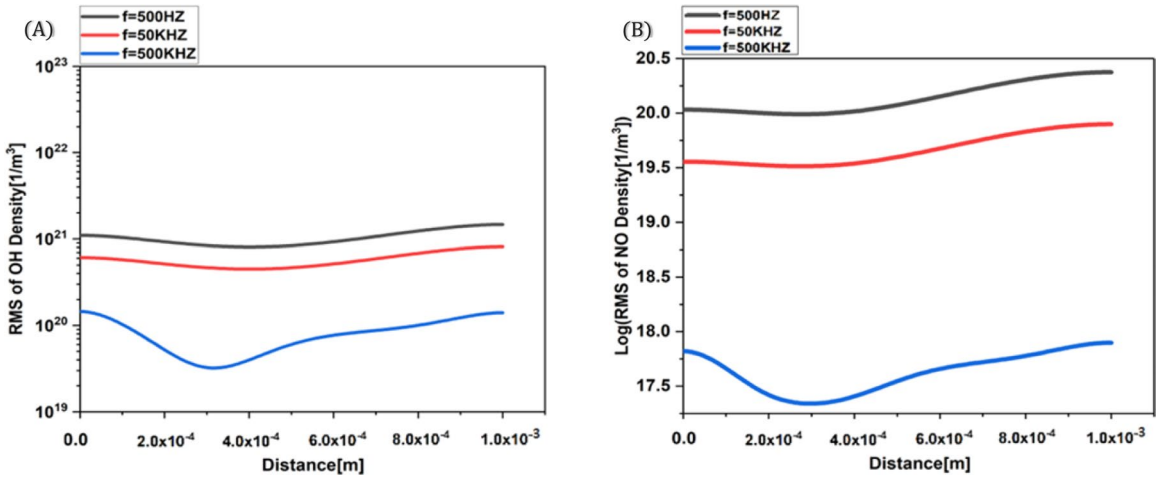

Fig. 8 The logarithmic RMS curve of the **A** OH and **B** NO species density distribution at three frequency levels in the plasma region

chemistry is shifting toward stronger ionization rather than dissociation.

3.2 Two-dimensional voltage distribution

The two-dimensional voltage distribution diagrams at three frequency levels are shown in Fig. 9.

In Fig. 9, the blue distribution represents the ground electrode, and the red distribution represents the power electrode. The horizontal axis shows the distance, the left vertical axis indicates the number of cycles, and the right vertical axis represents the voltage distribution.

3.3 Electric field distribution

In Fig. 10, the two-dimensional electric field shape illustrates that the field in the gap between the two electrodes is weaker than in the dielectric region, and this is due to the accumulation of surface charge, which tends to shield the electric field.

From a distance of −1 to 0, the electric field is within the dielectric range. The distance from 0 to 1 is the region where the plasma forms. Similarly, the distance from 1 to 2 is within the dielectric electric field. It should be noted that the dielectric region appears darker, whereas the plasma region is lighter. The reason for the breakdown of the electric field is the accumulation of surface charge on the dielectric surface. Another physical reason is that the field inside the dielectric is stronger than the field inside the plasma.

The quantity acquired for the species was contrasted with earlier research. Because the plasmas used in the previous research were specially designed for different objectives, the plasma's properties, such as voltage, were set at higher levels, which increased the discharge gap. Nonetheless, the density of particles is precisely proportional to the air atmospheric pressure plasma [25–27]. The electron density

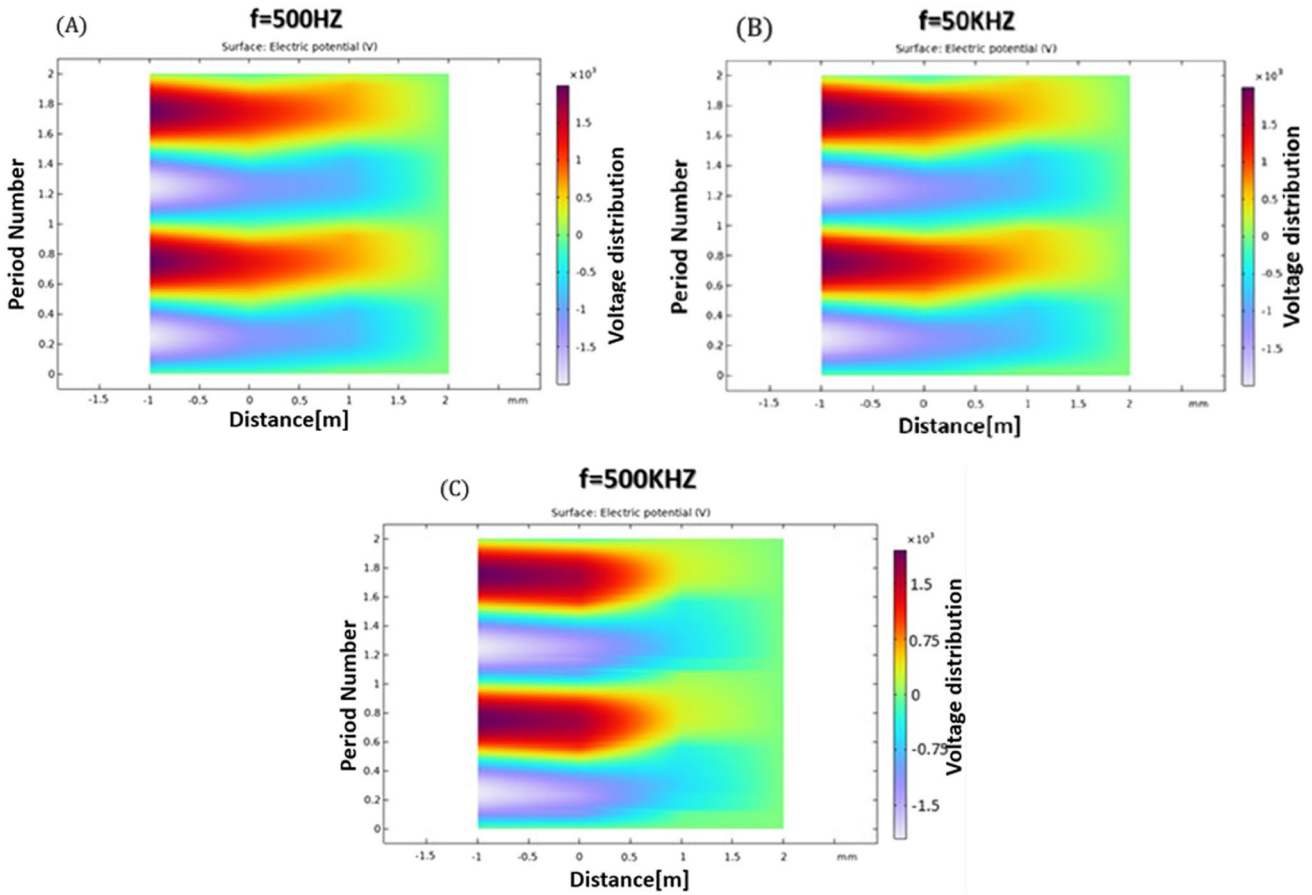

Fig. 9 The two-dimensional voltage distribution diagram at three frequency levels: **A** 500 Hz, **B** 50 kHz, and **C** 500 kHz

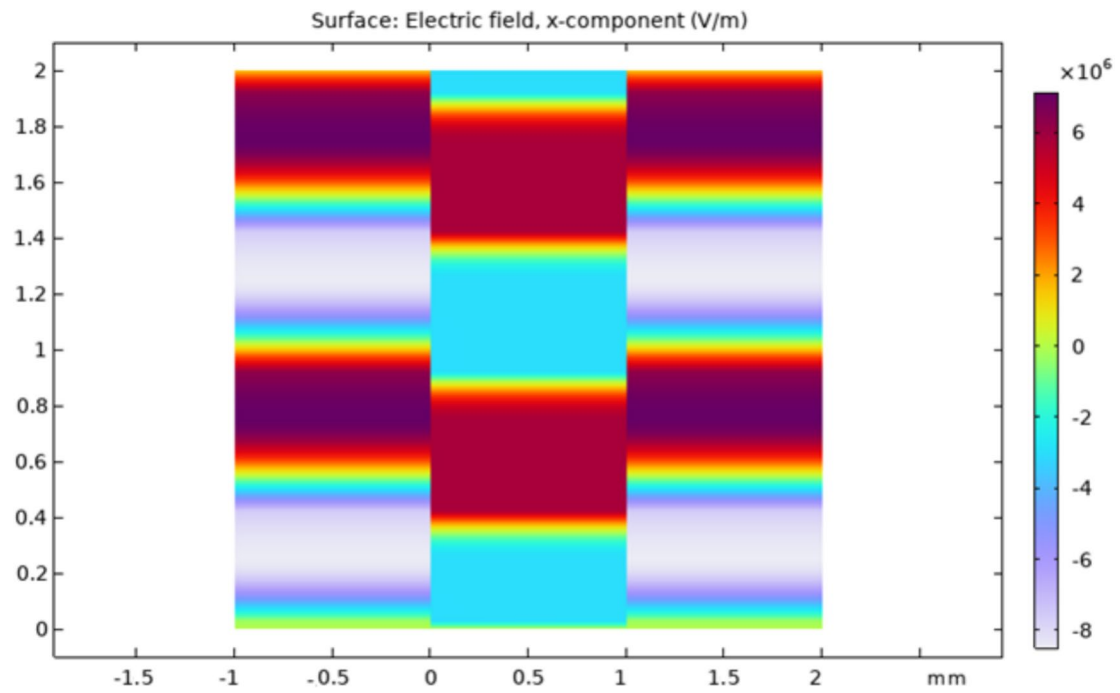

Fig. 10 Electric field distribution at a frequency of 50 kHz

obtained from our COMSOL simulation of DBD plasma is in close agreement with the values reported in [28]. In this overview, different methods used in plasma electron density measurement had been investigated. And they reported the electron density range 10^9–10^{18} ($1/cm^3$) which result obtained in this worked showed the same range [18, 29]. The electron temperature in simulation is 5.5 in maximum which is in the range. The electron temperature for air gas discharge is 2–10 eV depending on the input parameter [30, 31]. Effect of frequency on O3 generation efficiency had been investigated by Huang et al.[32]. The results indicate that ozone generation efficiency rises with increasing ozone concentration at 50 Hz: conversely, this efficiency declines with higher ozone concentration at 2.6 kHz and 20 kHz. Similarly, reference [33] showed a one-dimensional fluid model including 17 species and 65 reactions is used to investigate the effects of driving frequency on the generation and elimination of ROS in atmospheric radio frequency helium–oxygen discharges. The computational findings indicate that when frequency increases, the densities of ROS (atomic oxygen, ozone, excited atomic oxygen, and singlet delta oxygen) consistently drop at a fixed power density. Also, the study of the effect of frequency on temperature and electron density at radio frequencies (100 MHz) up to 2.45 GHz has been explained by Kwon et al. [34]. Moreover, importance of pulse repetition in air discharge had been investigated by Kushner et al. [35]. Although they used a numerical simulation with different parameters in comparison current work, the effect of frequency on RON's production is obvious.

The results show only minor discrepancies, which can be attributed to differences in model assumptions, boundary conditions, or numerical methods. This validation confirms the reliability of our simulation approach in accurately capturing the plasma behavior.

4 Conclusion

In this study, the electron temperature profile characteristic of this simulation was obtained and found to match the electron temperature profile derived from the experimental data in the previous articles. The results of the study demonstrate that the frequency of the applied voltage significantly influences the density of species generated in the atmospheric pressure gas discharge. Considering the impact of each species in various plasma applications, adjusting the frequency of the applied voltage can optimize and achieve the desired values under different conditions. These findings indicate that the density of ionized oxygen and nitrogen species increases with increasing applied frequency. Furthermore, the results showed that increasing the frequency of the applied voltage in gas discharge enables plasma generation at lower voltages while also altering the density of influential species, such as ozone density, oxygen atoms, and NOx species. Moreover, even with identical power consumption and applied voltage at different frequencies, observable variations are still present.

Acknowledgements This work was funded by the EU NextGenerationEU through the Recovery and Resilience Plan for Slovakia under Project No. 09I03-03-V03-00033 EnvAdwice, and Slovak Research and Development Agency APVV-22-0247.

Author contributions F.M. and H.S. wrote the main manuscript text; R.M.: preparation of structure and figures. F.S. reviewed the manuscript.

Data availability No datasets were generated or analyzed during the current study.

Declarations

Conflict of interest The authors declare no competing interests.

References

1. S. Kanazawa, M. Kogoma, T. Moriwaki, S. Okazaki, Stable glow plasma at atmospheric pressure. J. Phys. D Appl. Phys. **21**(5), 838 (1988). https://doi.org/10.1088/0022-3727/21/5/028
2. T. Yokoyama, M. Kogoma, S. Kanazawa, T. Moriwaki, S. Okazaki, The improvement of the atmospheric-pressure glow plasma method and the deposition of organic films. J. Phys. D Appl. Phys. **23**(3), 374 (1990)
3. P. Charipoor et al., Evaluation of voltage effect on FE-DBD plasma for skin treatment: biometrics analysis and hyperspectral investigation. Plasma Process. Polym. **21**(12), 2400148 (2024). https://doi.org/10.1002/ppap.202400148
4. A.L.W. Kelton, *Simulation Modeling and Analysis* (McGraw Hill, 2000)
5. J. Banks, *Discrete Event System Simulation* (Pearson Education India, 2005)
6. R. Mehrabifard, H. Mehdian, K. Hajisharifi, E. Amini, Improving cold atmospheric pressure plasma efficacy on breast cancer cells control-ability and mortality using vitamin c and static magnetic field. Plasma Chem. Plasma Process. **40**(2), 511–526 (2020). https://doi.org/10.1007/s11090-019-10050-5
7. R. Mehrabifard, H. Mehdian, M. Bakhshzadmahmodi, Effect of non-thermal atmospheric pressure plasma on MDA-MB-231 breast cancer cells. Pharm. Biomed. Res. **3**(3), 12–16 (2017). https://doi.org/10.29252/pbr.3.3.12
8. C.M. Banks, J.A. Sokolowski, *Modeling and Simulation Fundamentals: Theoretical Underpinnings and Practical Domains* (Wiley, 2010)
9. R. Mehrabifard, Z. Kabarkouhi, F. Rezaei, K. Hajisharifi, H. Mehdian, Physical insight into the synergistic enhancement of CAP therapy using static magnetic field. Braz. J. Phys. **54**(4), 1–10 (2024). https://doi.org/10.1007/S13538-024-01501-2
10. P.A. Fishwick, Simulation model design and execution: building digital worlds. IIE Trans. **28**(9), 778–780 (1996). https://doi.org/10.1080/15458830.1996.11770729
11. O. Ghazian, Numerical modeling of deformation, oscillation, spreading and collision characteristics of droplets in an electric field (2014). search.proquest.com.

12. U. Kogelschatz, B. Eliasson, W. Egli, Dielectric-barrier discharges. Principle and applications. Le J. Phys. **07**(C4), C4-47-C4-66 (1997). https://doi.org/10.1051/jp4:1997405
13. J.R. Roth, *Industrial Plasma Engineering: Volume 2: Applications to Nonthermal Plasma Processing*, vol. 2 (CRC Press, 2001), pp.1–628
14. Y.B. Golubovskii, V.A. Maiorov, J.F. Behnke, J.F. Behnke, Modelling of the homogeneous barrier discharge in helium at atmospheric pressure. J. Phys. D Appl. Phys. **36**(1), 39–49 (2003). https://doi.org/10.1088/0022-3727/36/1/306
15. D. Petrović, T. Martens, J. van Dijk, W.J.M. Brok, A. Bogaerts, Fluid modelling of an atmospheric pressure dielectric barrier discharge in cylindrical geometry. J. Phys. D Appl. Phys. **42**(20), 205206 (2009). https://doi.org/10.1088/0022-3727/42/20/205206
16. R. Abidat, S. Rebiai, L. Benterrouche, Numerical simulation of atmospheric dielectric barrier discharge in helium gas using COMSOL multiphysics. 2013 3rd International Conference on Systems and Control. ICSC 2013, pp. 134–139, (2013). https://doi.org/10.1109/ICOSC.2013.6750848
17. S. Gadkari, T.S.X. XinGuTu, Fluid model for a partially packed dielectric barrier discharge plasma reactor. Phys. Plasmas **24**, 93510 (2017). https://doi.org/10.1063/1.5000523
18. F. Sohbatzadeh, H. Soltani, Time-dependent one-dimensional simulation of atmospheric dielectric barrier discharge in N2/O2/H2O using COMSOL multiphysics. J. Theor. Appl. Phys. **12**(1), 53–63 (2018). https://doi.org/10.1007/s40094-018-0281-4
19. S. Hajikhani, R. Mehrabifard, H. Soltani Ahmadi, A numerical analysis of the impact of gas pressure and dielectric material on the generation of body force in an air gas plasma actuator. Radiat Phys Eng **5**(2), 51–60 (2024). https://doi.org/10.22034/rpe.2024.429773.1176
20. R. Mehrabifard, Two-dimensional simulation of argon dielectric barrier discharge (DBD) in plasma actuator structure with COMSOL multiphysics. SSRN Electron. J. **4**(4), 43–50 (2023). https://doi.org/10.2139/ssrn.4420891
21. Z. Soltani, R. Mehrabifard, F. Rezaei, M.M. Hatami, H. Soltani, Simulation of the impact of humidity on the species generated by a one-dimensional discharge of helium gas. J. Theor. Appl. Phys. **18**(3), 1–10 (2024). https://doi.org/10.57647/J.JTAP.2024.1803.39
22. LXCAT, Electron scattering database, University of Toulouse, France (2023). www.lxcat.net. Accessed 17 Dec 2023
23. P. L. Hagelaar GJM, BOLSIG+, electron Boltzmann equation solver (2023). https://www.bolsig.laplace.univ-tlse.fr. Accessed 17 Dec 2023
24. V.A. Godyak, R.B. Piejak, B.M. Alexandrovich, Electron energy distribution function measurements and plasma parameters in inductively coupled argon plasma. Plasma Sources Sci. Technol. **11**(4), 525–543 (2002). https://doi.org/10.1088/0963-0252/11/4/320
25. S. Dhungana, R.P. Guragain, H.B. Baniya, G.K. Chettri, G.P. Panta, D.P. Subedi, Effect of working gas and applied voltage on the estimation of power and electron density in gliding arc discharge (GAD) system. Jordan J. Phys. **16**(3), 321–327 (2023). https://doi.org/10.47011/16.3.7
26. F. Leipold, R.H. Stark, A. El-Habachi, K.H. Schoenbach, Electron density measurements in an atmospheric pressure air plasma by means of infrared heterodyne interferometry. J. Phys. D Appl. Phys. **33**(18), 2268–2273 (2000). https://doi.org/10.1088/0022-3727/33/18/310
27. O.V. Van Rooij, O. Ahlborn, A. Sobota, Electron density in a non-thermal atmospheric discharge in contact with water and the effect of water temperature on plasma-water interactions. J. Phys. D Appl. Phys. (2024). https://doi.org/10.1088/1361-6463/ad59b0
28. A.Y. Nikiforov, C. Leys, M.A. Gonzalez, J.L. Walsh, Electron density measurement in atmospheric pressure plasma jets: Stark broadening of hydrogenated and non-hydrogenated lines. Plasma Sources Sci. Technol. (2015). https://doi.org/10.1088/0963-0252/24/3/034001
29. R. Shrestha, E. Reeta Shilpakar, D. Prasad Subedi, Measurement of electron density in atmospheric pressure cold argon plasma jet. Int. J. Recent Res. Rev., XII, 2 (2019)
30. Y.J. Hong et al., Measurement of hydroxyl radical density generated from the atmospheric pressure bioplasma jet. J. Instrum. **7**(03), C03046 (2012). https://doi.org/10.1088/1748-0221/7/03/C03046
31. J.H. Kim, Y.H. Choi, Y.S. Hwang, Electron density and temperature measurement method by using emission spectroscopy in atmospheric pressure nonequilibrium nitrogen plasmas. Phys. Plasmas (2006). https://doi.org/10.1063/1.2338282/931098
32. G.M. Huang, T. Wang, I.V Timoshkin, S.J. Macgregor, M.J. Given, M.J. Wilson, Investigation of ozone generation using dielectric barrier discharges at 50 Hz, 2.6 kHz and 20 kHz. Gd2012, pp. 650–653 (2012)
33. Y.T. Zhang, J. He, Frequency effects on the production of reactive oxygen species in atmospheric radio frequency helium-oxygen discharges. Phys. Plasmas (2013). https://doi.org/10.1063/1.4775729/1016498
34. H.C. Kwon, I.H. Won, J.K. Lee, Electron heating mode transition induced by ultra-high frequency in atmospheric microplasmas for biomedical applications. Appl. Phys. Lett. (2012). https://doi.org/10.1063/1.4711207
35. S.A. Norberg, G.M. Parsey, A.M. Lietz, E. Johnsen, M.J. Kushner, Atmospheric pressure plasma jets onto a reactive water layer over tissue: pulse repetition rate as a control mechanism. J. Phys. D Appl. Phys. (2019). https://doi.org/10.1088/1361-6463/aae41e